Nonlinear Behavior of Helmholtz Resonator With a Compliant Wall for Low-Frequency, Broadband Noise Control

Maya Pishvar
Department of Mechanical and Aerospace Engineering,
The Ohio State University,
Columbus, OH 43210
e-mail: maya.pishvar@csun.edu

Ryan L. Harne[1]
Department of Mechanical Engineering,
The Pennsylvania State University,
University Park, PA 16802
e-mail: ryanharne@psu.edu

Low-frequency sound attenuation is often pursued using Helmholtz resonators (HRs). The introduction of a compliant wall around the acoustic cavity results in a two degrees-of-freedom (2DOF) system capable of more broadband sound absorption. In this study, we report the amplitude-dependent dynamic response of a compliant-walled HR and investigate the effectiveness of wall compliance to improve the absorption of sound in linear and nonlinear regimes. The acoustic-structure interactions between the conventional HR and the compliant wall result in non-intuitive responses when acted on by nonlinear amplitudes of excitation pressure. This paper formulates and studies a reduced order model to characterize the nonlinear dynamic response of the 2DOF HR with a compliant wall compared to that of a conventional rigid HR. Validated by experimental evidence, the modeling framework facilitates an investigation of strategies to achieve broadband sound attenuation, including by selection of wall material, wall thickness, geometry of the HR, and other parameters readily tuned by system design. The results open up new avenues for the development of efficient acoustic resonators exploiting the deflection of a compliant wall for suppression of extreme noise amplitudes. [DOI: 10.1115/1.4052870]

Keywords: dynamics, noise control, nonlinear vibration, structural acoustics

1 Introduction

Low-frequency noise may be radiated by various sources such as compressors, boilers, vehicles, ships, and aircraft. This poses a potential health hazard for humans, a nuisance for communication, or a concern for the integrity of structures [1,2]. Yet, elimination of such undesirable noise at the source may often not be feasible due to the complexities in the system design and implementation. Accordingly, the use of either passive or active noise control, including Helmholtz resonators (HRs), has attracted significant interest [3,4]. Conventional HRs, in which the air in the neck acts as an acoustic mass and the air expansion in the rigid-walled cavity represents a compliance, provide sound absorption by virtue of the resonant operational principle [5]. In this respect, Tang and Sirignano [6] investigated neck lengths for improved HR acoustic energy absorption. Moreover, various approaches have been presented to improve the attenuation of HRs, for example, by introducing tapered necks [7], variable-area and perforated extended necks [8], and spiral necks [9]. By another approach, Selamet et al. [10] partially filled an HR cavity with fibrous material and investigated the effect of the density and thickness of this material on the resonant behavior. While the conventional rigid HR is most effective over a narrow frequency range, recent efforts have been devoted to broaden the frequency range in addition to improving sound absorption capacity of HRs.

Tuning techniques including the integration of an active piezoelectric backplate in the HR are leveraged to adjust in real-time the resonant frequency [11,12]. In this technique, by changing the shunted electrical loads, the resonator volume changes, resulting in adaptive tuning of natural frequency and acoustic impedance. To avoid the cost and complexity associated with the active control techniques, serial and parallel assemblies of HRs have drawn attention, providing broadband resonant characteristics [13–17]. Yet, use of multiple HRs may not be feasible because of space constraints. In this respect, Hu et al. [18] revealed that the HR with an embedded soft structural membrane can generate multiple resonances in the low-frequency regime, achieving a better performance than traditional rigid HRs. In this system, the membrane element introduces an additional degree-of-freedom (DOF) to the HR and the coupling between elastic and acoustic physics allows for improved acoustic energy transfer [19]. A similar approach was adopted in Refs. [20,21], where a compliant diaphragm substitutes the rigid wall of a cylindrical HR to obtain an enhanced transmission loss and a shift in the resonance frequency.

In addition, Cui and Harne [22] leveraged a flexible structural member in an adaptive HR to control structural-acoustic coupling via controlled elastic buckling phenomena. While previous studies have illustrated the potential of HR with a compliant membrane for broadband absorption of sound in the condition of low pressure amplitude, i.e., linear regime [3,20,21], the assessment of amplitude-dependent dynamic response of compliant-walled HR is lacking. It is established that when the pressure amplitude level is high (greater than about 100 dB), sound absorption in conventional rigid HR is a function of pressure wave amplitude due to the nonlinear effects [23–25]. The nonlinear damping due to the jet loss and the nonlinear restoration (with quadratic and cubic term) coming from the nonlinear elasticity of the cavity air compression and rarefaction are the two primary sources of nonlinearity [23,26,27]. Thus, understanding the nonlinear acoustic-structure interaction in a compliant-walled HR is of importance for their use in low-frequency, broadband sound attenuation applications.

Motivated by the shortcomings in the state-of-the-art, this study develops, validates, and leverages a reduced order model derived from first principles to articulate the capability for compliant-walled HRs to capture nonlinear amplitude sound. The paper is organized as follows: in Sec. 2, a proof-of-concept HR with a single, compliant aluminum wall is developed and the effectiveness of wall compliance to improve the absorption of sound is investigated in linear

[1]Corresponding author.

Contributed by the Noise Control and Acoustics Division of ASME for publication in the Journal of Vibration and Acoustics. Manuscript received June 8, 2021; final manuscript received October 21, 2021; published online December 2, 2021. Assoc. Editor: Miao Yu.

and nonlinear regimes. In Sec. 3, governing equations of the coupled system are determined wherein the linear damping, nonlinear damping, nonlinear restoration, external excitation, and the effective mass, compliance, and damping of the flexible wall are taken into account. In Secs. 4 and 5, the model is first experimentally validated and then leveraged to investigate the interaction mechanisms between HR and compliant wall at various excitation amplitudes, resonator geometries, and wall materials that may give rise to unique noise attenuation capabilities. Finally, the paper is concluded in Sec. 6 with a summary of the knowledge gained.

2 Helmholtz Resonator Composition and Experimental Setup

In this work, the acoustic-structure interaction between the HR and a compliant wall is studied. The experimental setup in Figs. 1(*a*) and 1(*b*) is used to examine the resonant frequency of the HR with rigid walls or when one wall is replaced with the compliant aluminum structure. The HR with five square walls enclosing a cubic inner cavity having a volume of $V_1 = 0.0153\ \text{m}^3$ is fabricated from 1.9 cm thick, rigid medium-density fiber (MDF) board. The front wall of the HR has a square opening (side length $b = 0.13$ m) marked by the square in Figs. 1(*a*) and 1(*b*). Either a rigid 1.9 cm thick MDF wall is installed in this square window or the compliant aluminum wall with thickness 30 μm is installed. The necks for tuning the length of the cylindrical opening are made by 3D printing ABS plastic (FlashForge Creator Pro). The experimental setup includes an electrodynamic shaker (LDS V408) attached to a square MDF piston (side length 0.17 m), where the movement of the piston acts as an excitation for the HR system. The resonator is placed on an aluminum truss above the piston so that the HR side walls are sealed with rubber to the piston. In the low-frequency range considered in this work, the acoustic wavelength is much larger than the side lengths of the inner cavity. As a result, the acoustic pressure inside HR is uniform, measured by a microphone (PCB 130E20), inserted into the HR cavity and secured to the HR side wall. To determine the acceleration of the piston, the accelerometer (PCB 333B40) is mounted on top of piston. A feedback-based vibration controller (Vibration Research, VR9500) electronically governs the shaker piston acceleration. The shaker is excited with constant acceleration so that in the free field, the piston would drive a constant sound pressure level (SPL) at all frequencies. At large amplitude excitations, the effects of the nonlinearities may notably influence the acoustic behavior of the HR. Thus, the HR was subjected to excitation acceleration amplitudes from 0.1 m/s^2 to 6 m/s^2 to assess the effectiveness of wall compliance to improve the absorption of sound in both linear and nonlinear regimes. To compare the influence of neck length on the structural-acoustic responses, three neck lengths are considered, $L = 0.035$, 0.075, and 0.115 m each with a neck radius dimension of $a = 0.02$ m.

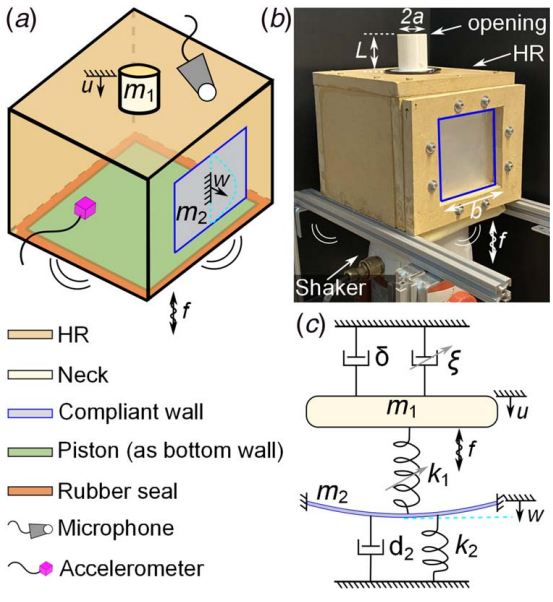

Fig. 1 (*a*) Schematic and (*b*) photograph of the setup for measuring the resonant frequency of experimental HR. The compliant aluminum or rigid MDF wall is installed at the position marked by the square, with side length of *b*. (c) Schematic of the lumped parameter model of the HR with one compliant wall.

3 Analytical Modeling of Resonator With Compliant Wall

The schematic of the nonlinear HR with a compliant wall investigated in this paper is presented in Fig. 1(*c*). The governing equations of motion for the HR assembly are derived in the following. The governing equation of motion for the air mass m_1 and displacement u in the resonator neck is derived by Newton's second law. Here, we consider nonlinear compression of the air in enclosed chamber, nonlinear aerodynamic loss by viscous motion of air in the neck, linear radiation damping, as well as external pressure excitation. The resulting single DOF equation of motion is given in Eq. (1) [23,28,29].

$$m_1\ddot{u} + \delta\dot{u} + \xi\dot{u}|\dot{u}| + \Delta P_{\text{cav}}A_1 = f(t) \tag{1}$$

Here, the air mass in the neck is $m_1 = \rho_1 L_{1e} A_1$, where ρ_1 is the density of air, A_1 is the cross section of the straight neck, and L_{1e} is the effective length of neck. The effective length of the neck accounts for the outer and inner opening of the neck whether both ends are flanged or unflanged, with the approximation of $L_{1e} = L + (16a/3\pi)$ for the case of both ends flanged, where L is the geometric neck length and a is the radius of the neck [30]. The coefficient for linear damping is $\delta = \delta^* m_1$, where $\delta^* = (A_1/\rho_1 L_{1e})\text{Re}\{Z_{\text{in}} + Z_{\text{vis}}\}$, in which Re represents the real part of a complex variable [24]. The Z_{in} is the acoustic impedance at the inlet of the HR and Z_{vis} is the impedance of the acoustic friction. The nonlinear damping accounts for the force due to the acceleration of air from the external pulsating system into the neck [26]. The nonlinear damping coefficient is $\xi = \xi^* m_1/2L_{1e}$, where ξ^* is the total hydraulic resistance coefficient of the neck. Thus, with a proper choice of ξ^*, a mean-flow pressure drop in the neck, produced by boundary layer friction, is considered [26]. The $f(t) = P(t)A_1$ is the applied harmonic acoustic force to the neck from the exterior.

The restoring force to return the air mass to equilibrium originates from the compressibility of air enclosed in the cavity. The change in the volume of the cavity $\Delta V = -\left(A_1 u - \int w dA_2\right)$ is due to the displacement u of the air in the neck and deflection w of a plate with area of A_2, resulting in an approximate condensation of $\Delta\rho/\rho_1 = -\Delta V/V_1 = (u - \psi w)A_1/V_1$. Here, the coefficient ψ can be approximated by the ratio of area of flexible plate to that area of neck.

When the excitation SPL is high, the nonlinear pressure change ΔP_{cav} (in the acoustic approximation) caused by the finite distortion of the air in the cavity is expanded in Taylor's series approximation using [23–25]

$$\Delta P_{\text{cav}} = \rho_1 L_{1e}\omega_1^2\left[(u - \psi w) - \frac{(\gamma+1)A_1}{2V_1}(u - \psi w)^2 + \frac{(\gamma+1)(\gamma+2)A_1}{6V_1^2}(u - \psi w)^3\right] \tag{2}$$

Here, V_1 is the undisturbed volume in the cavity, γ is the specific heat ratio of the air, and $\omega_1 = \sqrt{k_1/m_1}$ is the linear resonant

frequency of the resonator considering linear acoustic stiffness $k_1 = \rho_1 c_1^2 A_1^2 / V_1$ with sound speed c_1.

Equation (2) is substituted into Eq. (1) to yield Eq. (3).

$$m_1\ddot{u} + \delta\dot{u} + \zeta\dot{u}|\dot{u}| + m_1\omega_1^2\left[(u-\psi w) - \frac{(\gamma+1)A_1}{2V_1}(u-\psi w)^2 + \frac{(\gamma+1)(\gamma+2)A_1}{6V_1^2}(u-\psi w)^3\right] = p(t)A_1 \tag{3}$$

The compliant wall is modeled as a thin, flexible panel. The compliant wall vibrates in the lowest order mode due to uniform-phase pressure applied over the surface that interfaces with the cavity. The equation of motion for the displacement w of the lowest order modal mass m_2 of the compliant panel is derived by Newton's second law.

$$m_2\ddot{w} + d_2\dot{w} + k_2 w - m_1\omega_1^2\psi\left[(u-\psi w) - \frac{(\gamma+1)A_1}{2V_1}(u-\psi w)^2 + \frac{(\gamma+1)(\gamma+2)A_1}{6V_1^2}(u-\psi w)^3\right] = 0 \tag{4}$$

The mass contribution to the lowest order vibration of the flexible plate is obtained by $m_2 = \Lambda\rho_2 V_2$, where ρ_2 and V_2 are the flexible plate density and volume, respectively. The $\Lambda = 0.25$ chosen in this study is obtained from Refs. [31,32]. The lowest order, in-vacuo natural frequency of the square panel is $\omega_2 = (\lambda/m_2 b^2)\sqrt{D/\rho_2}$. The vibration frequency factor λ is tabulated by Leissa [33] based on the panel boundary conditions and aspect ratio. Here, we consider a square compliant wall plate with clamped edges, having length and width b, and thickness h. The bending stiffness, D, is determined by the isotropic Young's modulus E, Poisson's ratio ν, and thickness h of the flexible plate, i.e., $D = Eh^3/[12(1-\nu^2)]$. Using the equivalent relation $\omega_2 = \sqrt{k_2/m_2}$, the stiffness of the lowest order plate bending mode k_2 is computed.

The relative displacement between the air and compliant wall is defined to be $z = u - \psi w$. By substitution, Eqs. (5) and (6) are obtained.

$$\ddot{u} + \frac{\delta}{m_1}\dot{u} + \frac{\xi^*}{2L_{1e}}\dot{u}|\dot{u}| + \omega_1^2\left[z - \frac{(\gamma+1)A_1}{2V_1}z^2 + \frac{(\gamma+1)(\gamma+2)A_1}{6V_1^2}z^3\right] = \frac{p(t)}{\rho_1 L_{1e}} \tag{5}$$

$$\ddot{u} - \ddot{z} + \frac{d_2}{m_2}(\dot{u}-\dot{z}) + \frac{k_2}{m_2}(u-z) - \frac{m_1}{m_2}\psi^2\omega_1^2\left[z - \frac{(\gamma+1)A_1}{2V_1}z^2 + \frac{(\gamma+1)(\gamma+2)A_1}{6V_1^2}z^3\right] = 0 \tag{6}$$

The time is non-dimensionalized by $\tau = \omega_1 t$ so that $(\,)' = \partial/\partial\tau$. Also, $u^* = A_1 u/V_1$ and $z^* = A_1 z/V_1$. The mass ratio is defined to be $\mu = m_1/m_2$. The frequency ratio is $f = \omega_1/\omega_2$. We also define $\xi_1 = \delta^*/\omega_1$, $\xi_2 = d_2 m_2/\omega_2$, and $\eta_a = (\xi^*/2)V_1/A_1 L_{1e}$. The nonlinear pressure coefficients are defined as $\alpha_2 = (\gamma+1)/2$ and $\alpha_3 = (\gamma+1)(\gamma+2)/6$. The harmonic applied pressure is $p(t) = p_0\cos\Omega t$. The normalized applied pressure amplitude is $P = p_0/\rho_1 c_1^2$. The non-dimensional excitation frequency is given to be $\omega = \Omega/\omega_1$. Thus, the non-dimensional equations of motion are as follows:

$$u'' + \xi_1 u' + \eta_a u'|u'| + [z - \alpha_2 z^2 + \alpha_3 z^3] = P\cos\Omega t \tag{7}$$

$$f^2(z''-u'') + \xi_2 f(z'-u') + (z-u) + f^2\mu\psi[z - \alpha_2 z^2 + \alpha_3 z^3] = 0 \tag{8}$$

where for simplification, the asterisk * is omitted. In this research, harmonic response is assumed for the lowest order behaviors of the structural-acoustic system, presuming the wavelengths are much greater than any physical dimension of the HR. Solutions to Eqs. (7) and (8) are assumed of the form

$$u(t) = x_1(t) + x_2(t)\sin(\omega t) + x_3(t)\cos(\omega t) \tag{9}$$

$$z(t) = x_1(t) + x_4(t)\sin(\omega t) + x_5(t)\cos(\omega t) \tag{10}$$

Given that $z = u - \psi w$, the approximation of the response $w(t)$ is

$$w(t) = (1/\psi)[(x_2(t) - x_4(t))\sin(\omega t) + (x_3(t) - x_5(t))\cos(\omega t)] \tag{11}$$

The attached compliant wall does not have a constant term in the expansion due to the notation that w represents a relative coordinate. Equations (9) and (10) are substituted into (7) and (8). Then the higher order harmonics are neglected, the constant, $\sin(\omega t)$, and $\cos(\omega t)$ terms are grouped, and the unknown, time-varying coefficients are presumed to change slowly $x_1' \approx 0$, $x_2' \approx 0$, $x_3' \approx 0$, $x_4' \approx 0$, $x_5' \approx 0$. These operations and assumptions yield five governing equations for coefficients x_1, x_2, x_3, x_4, x_5:

$$\xi_1 x_1' = -\alpha_3 x_1^3 + \alpha_2 x_1^2 - \left(1 + \frac{3}{2}\alpha_3(x_4^2 + x_5^2)\right)x_1 + \frac{1}{2}\alpha_2(x_4^2 + x_5^2) \tag{12}$$

$$2\omega x_3' - \xi_1 x_2' = -\omega^2 x_2 - \xi_1\omega x_3 - \frac{8}{3\pi}\omega^2\eta_a x_3\sqrt{x_2^2 + x_3^2} + \left(1 - 2\alpha_2 x_1 + 3\alpha_3 x_1^2 + \frac{3}{4}\alpha_3 x_5^2\right)x_4 + \frac{3}{4}\alpha_3 x_4^3 \tag{13}$$

$$-2\omega x_2' + \xi_1 x_3' = -P + \xi_1\omega x_2 - \omega^2 x_3 + \frac{8}{3\pi}\omega^2\eta_a x_2\sqrt{x_2^2 + x_3^2} + \left(1 - 2\alpha_2 x_1 + 3\alpha_3 x_1^2 + \frac{3}{4}\alpha_3 x_4^2\right)x_5 + \frac{3}{4}\alpha_3 x_5^3 \tag{14}$$

$$f\xi_2 x_2' - 2f^2\omega x_3' - f\xi_2 x_4' + 2f^2\omega x_5' = (-1 + f^2\omega^2)x_2 + f\xi_2\omega x_3 + (1 + f^2\mu\psi^2 - f^2\omega^2 - 2f^2\alpha_2\mu\psi^2 x_1 + 3f^2\alpha_3\mu\psi^2 x_1^2)x_4 + \frac{3}{4}f^2\alpha_3\mu\psi^2 x_4^3 - f\xi_2\omega x_5 + \frac{3}{4}f^2\alpha_3\mu\psi^2 x_4 x_5^2 \tag{15}$$

$$f\xi_2 x_3' + 2f^2\omega x_2' - f\xi_2 x_5' - 2f^2\omega x_4' = (-1 + f^2\omega^2)x_3 - f\xi_2\omega x_2 + (1 + f^2\mu\psi^2 - f^2\omega^2 - 2f^2\alpha_2\mu\psi^2 x_1 + 3f^2\alpha_3\mu\psi^2 x_1^2)x_5 + \frac{3}{4}f^2\alpha_3\mu\psi^2 x_5^3 + f\xi_2\omega x_4 + \frac{3}{4}f^2\alpha_3\mu\psi^2 x_5 x_4^2 \tag{16}$$

Table 1 Experimental and model results comparison

		Model predictions			Experimental measurements		
Backwall	Length of HR neck (m)	Excitation SPL (dB)	Max SPL (dB)	Resonance frequency (Hz)	Acceleration (m/s^2)	Max SPL (dB)	Resonance frequency (Hz)
MDF	0.115	80	80	33	0.1	91	36
		100	100	32	2	116	33
		120	120	31	4	120	30
		140	140	29	6	122	27
		160	158	18	–	–	–
MDF	0.035	120	122	52	3	113	41
	0.075	120	121	40	3	118	37
	0.115	120	120	31	3	120	33
30-μm-thick aluminum	0.035	120	127	34	3	114	28
	0.075	120	125	28	3	118	24
	0.115	120	124	23	3	119	21

The steady-state responses of the system are determined by solving the coupled equations (12)–(16). As such, the five coefficients x_1, x_2, x_3, x_4, x_5 are obtained by simultaneously solving nonlinear equations (12)–(16), using a nonlinear least-squares minimization approach in MATLAB.

After acquiring the coefficients from Eqs. (12)–(16), the SPL inside the HR at each frequency is obtained

$$\mathrm{SPL} = 20\log_{10}\left|\rho_1 c_1^2\left(x_1 + \sqrt{x_2^2 + x_3^2}\right)\Big/\sqrt{2}/(20\times 10^{-6})\right| \quad (17)$$

The transfer function (TF) is predicted as the amplitude of the acoustic pressure inside the HR (SPL) to that of applied acoustic pressure.

4 Experimental Validation of the Analytical Model

An experimental validation of the analytical model is undertaken. A comparison between experimental and predicted results of the resonance frequency of the HR is presented in Table 1. The influences of change in excitation amplitude to result in the linear and nonlinear regimes as well as the effects of neck length (0.035, 0.075, 0.115 m) and wall compliance (i.e., rigid MDF or 30-μm-thick complaint aluminum) are assessed. In the following investigation, we use the material properties and empirical parameters given in Table 2 unless otherwise indicated. For modeling the MDF HR, the walls are assumed to be sufficiently rigid so that the physical properties and the thickness of the walls do not affect the resonator behavior. To predict linear as well as nonlinear acoustic behavior of the rigid HR, excitation SPLs of 80–160 dB are considered. To replicate this transition from linear to nonlinear regime experimentally, the excitation acceleration amplitudes are varied from 0.1 to 6 m/s^2, thus generating SPLs inside the HR from 91 to 122 dB. Note that the dissimilarity between the internal experimental SPL values with the external modeled SPL values is associated with the difference between the driving mechanisms of the fabricated HR and the modeled HR. In this low-frequency range of consideration, the sound pressure amplitude of 140 or 160 dB could not be achieved experimentally for comparison with the predicted ones because of the displacement limit of the shaker.

Table 2 Physical and empirical parameters for modeling

ρ_{air}(kg/m^3)	c_{air}(m/s)	γ
1.2	343	1.4
$E_{aluminum}$(GPa)	$\rho_{aluminum}$(kg/m^3)	$\nu_{aluminum}$
81	2710	0.33
E_{cork}(GPa)	ρ_{cork}(kg/m^3)	ν_{cork}
0.03	168	0.1
$E_{silicone}$(GPa)	$\rho_{silicone}$(kg/m^3)	$\nu_{silicone}$
0.01	1552	0.49
E_{epoxy}(GPa)	ρ_{epoxy}(kg/m^3)	ν_{epoxy}
3.7	1330	0.33
E_{CFRP}(GPa)	ρ_{CFRP}(kg/m^3)	ν_{CFRP}
111	1552	0.1
E_{steel}(GPa)	ρ_{steel}(kg/m^3)	ν_{steel}
228	8240	0.1
ξ	ψ	
1.87	1	

Table 1 shows that the model that predicts the resonance frequency of the conventional rigid HR reduces from 33 to 18 Hz when the excitation increases, from 120 to 160 dB, sufficiently to drive the HR into a nonlinear acoustic regime. Moreover, under the excitation SPL of 120 dB, the 8 cm increase in neck length results in the decrease in resonance frequency of conventional HR from 52 to 31 Hz. Yet, for the HR with a compliant aluminum wall, the reduction in resonance frequency is less, from 34 to 23 Hz, with the same increase in neck length. Considering the experimental data, the resonance frequency reduction trends predicted by the model for increasing nonlinearity, increasing neck length, and introduction of compliant wall are in qualitative agreement with the experimental findings. The discrepancies may result from the choice of empirical effective length of the neck L_{1e}, loss coefficient $\xi = 1.87$ which corresponds exactly to the geometrical length [26], and the ideal approximation of the compliant wall to be a thin, flexible panel in the model. The discrepancy can be compensated using separate expressions for effective length of the neck and nonlinear damping coefficients to represent the linear, nonlinear transition, and highly nonlinear regimes. Several correction factors are presented in earlier studies [34,35]. The model also shows that the max SPL increases with decreasing neck length, which is due to decreased losses, while in experiment, max SPL decreases because of reduced flow resistance. Yet, the overall agreement of salient trends is sufficient justification to further explore the model to help uncover the nonlinear acoustic-structure interaction mechanisms in a compliant-walled HR.

Furthermore, it is seen that the alteration in resonance frequency with replacement of one rigid wall with compliant wall occurs due to the creation of a 2DOF system. This influence is considerable in the low-frequency range. For instance, for each of the three neck lengths, when the excitation SPL is 120 dB, the resonance frequency of the HR with one compliant aluminum wall is estimated to be 26–35% lower than that of HR with rigid walls, which is similar to the 32–36% measured in the experiments. This demonstrates that the HR with a compliant wall can have a potential application for low-frequency noise control. Such an outcome is especially beneficial when space limits large HR cavities, which is a common way to reduce the frequency of resonance while maintaining effective inertial force of air. This shows the importance of an inclusive model that takes into account the important sources of

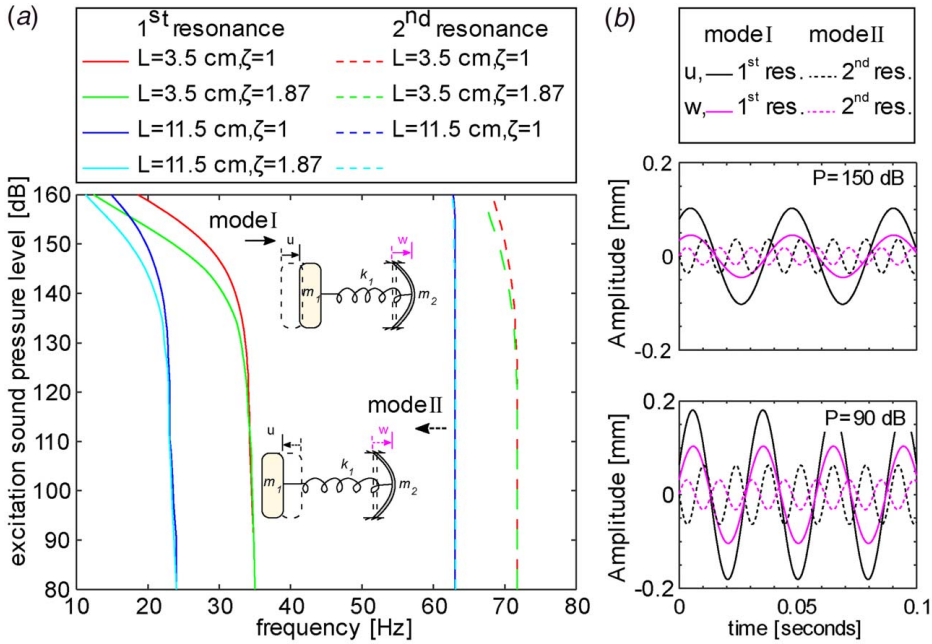

Fig. 2 Predictions of (*a*) first and second resonance of HR with compliant wall when the excitation increases from 80 dB to 160 dB, showing the influence of nonlinear damping as well as neck length with increasing P. Solid curves indicate the first resonance and dashed curves are the second resonance. Schematics showing the corresponding mode shapes, "mode I" and "mode II", of vibration of the HR assembly at first and second resonance. (*b*) Displacement amplitude for air in the neck, *u*, and compliant wall, *w*, as a function of time when the excitation SPL is 90 dB and 150 dB, at $L = 0.035$ m and $\xi = 1.87$.

nonlinearity as well as the dynamics between compliant wall and HR in order to accurately predict the resonator behavior.

5 Acoustic-Structure Interaction Phenomena in a Compliant-Walled Helmholtz Resonator

5.1 Resonant Behavior in Linear and Nonlinear Regimes. To develop an understanding of the nonlinear dynamics of the HR with compliant wall, we leveraged the analytical formulation to show in Fig. 2(*a*) the effects of nonlinear damping ($\xi = 1$ and 1.87) as well as neck length (0.035 and 0.115 m) on acoustic characteristics of HR. The natural frequency of rigid HR is 60 Hz for $L = 0.035$ m and 41 Hz for $L = 0.115$ m and the lowest order natural frequency of a flexible aluminum panel is approximated to be 42 Hz. In the coupled compliant-walled HR system, due to the presence of the 2DOF, there are two resonance peaks. The first and second resonance frequencies are illustrated in Fig. 2(*a*) by solid and dashed curves, respectively. It is found that at low SPL of 80 dB, the resonant frequencies of the primary two vibration modes are 24 and 63 Hz for $L = 0.115$ m and 35 and 72 Hz for $L = 0.035$ m. Figure 2(*a*) presents that when the excitation increases from 80 dB to 160 dB, where the nonlinearity plays a more significant role, the resonant frequencies of both peaks shift toward lower frequencies gradually. Yet, the first TF resonant peak is more sensitive to the amplitude of the excitation pressure.

The nonlinear damping is the nonlinear separation effect for the air flow in and out of the neck. In other words, $\xi = 1$ corresponds to a loss free inlet with a static pressure drop of one dynamic head across the neck inlet [26]. Figure 2(*a*) depicts that for high SPL, at a certain neck length, a higher nonlinear damping of $\xi = 1.87$ [24] leads to greater reduction in the resonance frequencies than those of $\xi = 1$, showing that nonlinear damping plays an important role in the design and tuning of a compliant-walled HR. One possible approach to reduce the loss coefficient and thus nonlinear damping is to replace the sharp edges of the neck with flared or tapered neck ends having a moderate arc, which may suppress flow separation [26]. Figure 2(*a*) also illustrates the nonlinear behavior of the reduction in resonance frequency with changing neck length. Especially, at high SPL, with a shorter neck, having a higher nonlinear damping may result in a more significant shift in resonance frequencies.

The corresponding mode shapes of the HR assembly at the first and second eigenfrequencies are determined from the positions of the air mass in the neck, *u*, and compliant wall, *w*. The resulting mode shapes are schematically demonstrated in Fig. 2(*a*). It can be seen that the motions of the air mass in the neck and compliant wall are in-phase at mode I, while it changes to 180 deg out-of-phase at mode II. Figure 2(*b*) shows the displacement amplitude of air mass in the neck and compliant wall as a function of time at modes I and II when the excitation SPL is 90 dB and 150 dB. At mode I, when the excitation increases from 90 dB to 150 dB, the ratio of amplitude of displacements $|u|/|w|$ increases from 1.7 to 2.3, respectively. This indicates that in the nonlinear regime, the displacement amplitude of air mass in the neck is more affected by the degree of nonlinearity than that of complaint wall. This may be expected because the compliant structural nonlinearity is not modeled, while nonlinearity is included for the air compression. Also, the compliant wall is not directly subjected to applied pressure unlike the air in the neck.

5.2 Assessment of Helmholtz Resonator Geometrical Features. To achieve a particular resonant frequency or configuration of two resonant peaks, the influence of geometrical features of HR on the TF amplitude of the acoustic pressure inside the HR to the acoustic excitation pressure is investigated at excitation SPL of 140 dB. Figure 3(*a*) presents the effect of neck opening radii *a* of 0.01, 0.02, and 0.03 m on the TF amplitude frequency response for both the conventional rigid and compliant-walled HRs. In conventional rigid HR, only one resonance peak arises which can be leveraged for acoustic energy absorption. Yet, the 2DOF coupled HR generates two TF resonant peaks, where the second peak

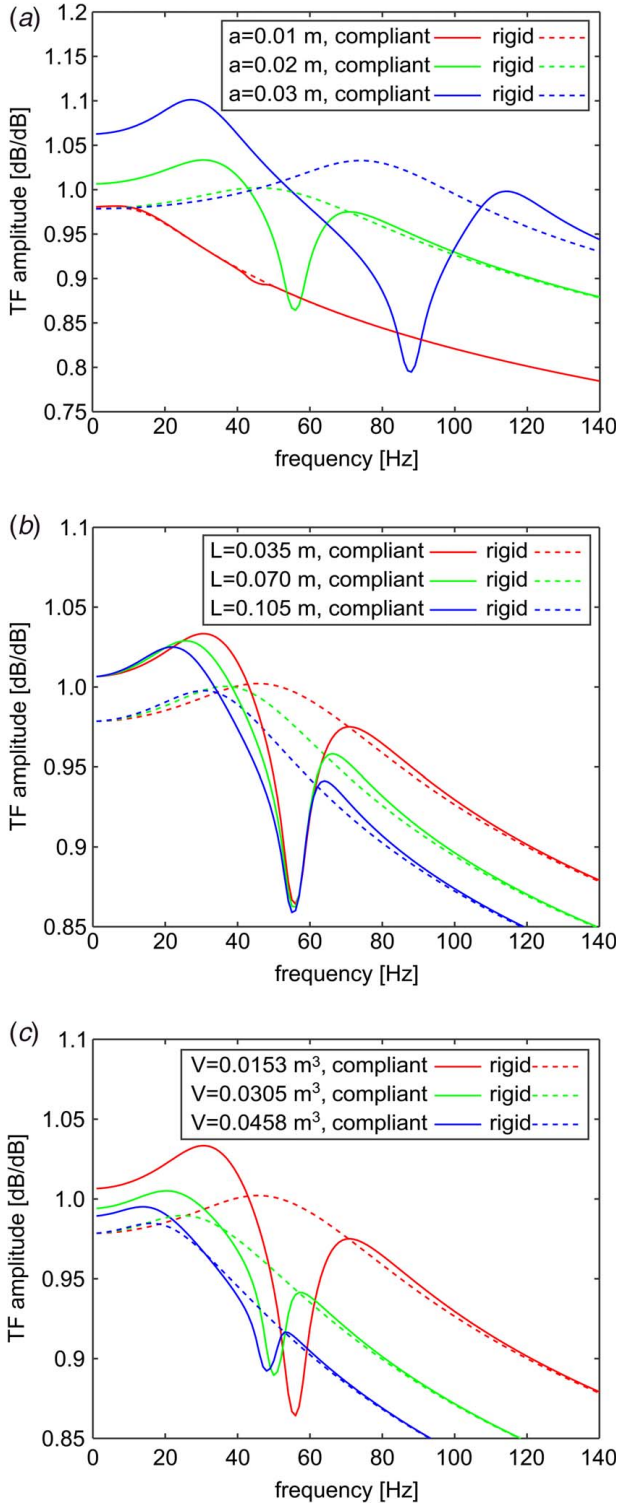

Fig. 3 Predictions of TF amplitude for (*a*) neck opening radii (a = 0.01, 0.02, and 0.03 m), (*b*) neck lengths (L = 0.035, 0.070, and 0.105 m), and (*c*) cavity volumes (V_1 = 0.0153, 0.0305, 0.0458 m^3) at SPL of 140 dB. Compliant-walled HR is indicated by solid curves, and conventional rigid HR are shown by the dashed curves. Unless otherwise mentioned, we use a = 0.02 m, L = 0.035 m, and V_1 = 0.0153 m^3.

vanishes for small neck radius, as shown in Fig. 3(*a*). Thus, compared to the 1DOF system, the 2DOF system enabled with introduction of one compliant wall may be more effective and adaptable for noise attenuation. The reason that smaller neck radii exhibit one resonance is that the stiffness from the air enclosed in the cavity decreases substantially while the stiffness of the compliant wall remains the same. This has the effect of separating the two modes by a large margin and minimizing coupling to excite the second mode that is predominantly composed of compliant wall vibration.

Furthermore, a valley between the two resonance peaks is evident due to the anti-resonance. Anti-resonance occurs when the inertial force generated by the compliant wall cancels the effects of external force. Figure 3(*a*) also depicts that at neck opening radius a of 0.03 m, the 1DOF rigid HR system has a TF resonant peak near 75 Hz, and the compliant-walled HR have two resonant peaks at 28 and 115 Hz. Moreover, the amplitude of TF peak at the first resonance frequency is more than that of 1DOF rigid HR because the change in volume of air in the cavity of the compliant-walled HR system is more than that of rigid HR. Similar to the rigid HR, with increasing neck radius, the magnitude of the resonance peak increases due to the increase in the air mass in the neck and a reduction in air flow resistance. Yet, unlike the rigid HR that the resonance frequency increases constantly, in 2DOF HR system, the first resonance frequency increases with increasing neck radius to a = 0.02 m, and then decreases with increasing neck radius to a = 0.03 m. The reason is that in compliant-walled HR, increasing neck radius has a dual effect. On one hand, it increases the air spring stiffness which increases the Helmholtz resonant frequency. On the other hand, increasing air spring stiffness improves the deflection of the flexible wall, which reduces the resonant frequency of the system. It should be noted that in the compliant wall HR, the attenuation bandwidth of the compliant wall HR is largely dictated by the resonance and anti-resonance frequencies. Thus, obtaining a wider effective bandwidth of compliant wall HR which corresponds to a broader attenuation curve compared to rigid HR is possible when the compliant wall HR system parameters are chosen properly.

Figure 3(*b*) shows the influence of neck lengths L of 0.035, 0.070, and 0.105 m on the TF amplitude frequency response for both the conventional rigid and compliant-walled HRs. Similar to the rigid HR where it is observed that the TF resonant peak decreases with increasing neck length, both resonant peaks for the coupled HR reduce due to the increased air flow resistance. Moreover, regardless of the introduction of wall compliance, the shorter neck provides a wider band of attenuation. A similar trend was found in the measured transmission loss for rigid HRs with neck extensions [8]. Furthermore, a greater shift in the resonance frequency is evident for the conventional rigid HR than for the coupled HR considering the same increase in neck length.

Figure 3(*c*) compares the influence of cavity volumes (V_1 = 0.0153, 0.0305, 0.0458 m^3) on the TF amplitude frequency response for both the conventional rigid and compliant-walled HRs. With increasing cavity volume, the magnitudes of the TF resonant peaks and the resonance frequencies reduce for all cases considered due to decrease in stiffness of air in the cavity. Tripling the cavity volume can reduce the resonance frequency in the 1DOF system by almost 30 Hz, while in the 2DOF HR system less reduction, approximately by 15 Hz, in resonance frequency may be seen. This may be expected because the change in acoustic stiffness of the cavity in the coupled HR is less than that of the rigid HR.

5.3 Effects of Frequency Ratio and Mass Ratio. To achieve a deeper insight on the interactions between acoustic and elastic physics in the 2DOF HR system, the effects of frequency ratio and mass ratio, exhibiting the coupling between HR and compliant wall, on the TF amplitude are presented in Fig. 4. Frequency tuning ratio of the resonator to the flexible plate is f, while the mass ratio of the acoustic mass in the neck to the mass contribution of flexible plate is μ. The color gradation varies from the solid hue for f = 2.0 (in Fig. 4(*a*)) or μ = 2.0 (in Fig. 4(*b*)) to light shading for f = 0.01 (in Fig. 4(*a*)) or μ = 0.01 (in Fig. 4(*b*)). To generate the results of Fig. 4, the parameters for HR assembly are selected to be a = 0.02 m, L = 0.035 m, V_1 = 0.0153 m^3, μ = 0.3 (in Fig. 4(*a*)), and f = 0.8 (in Fig. 4(*b*)) at SPL of 140 dB. As predicted,

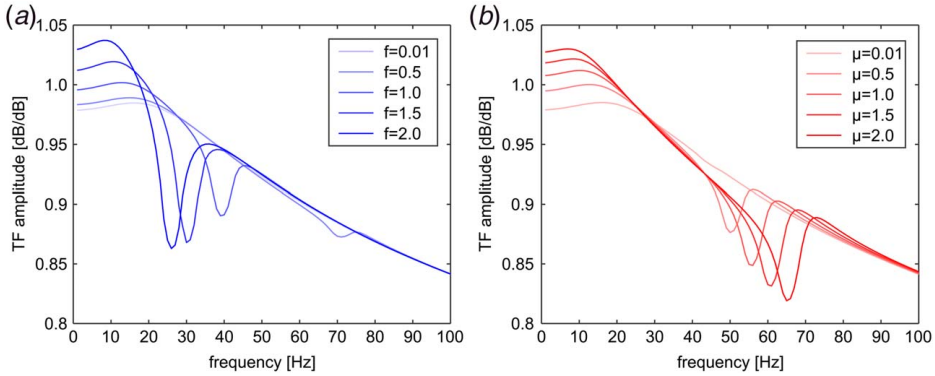

Fig. 4 Predictions of TF amplitude frequency response of compliant-walled HR at various (*a*) frequency ratios ($f = 0.01$, $f = 0.5$, $f = 1.0$, $f = 1.5$, and $f = 2.0$) and (*b*) mass ratios ($\mu = 0.01$, $\mu = 0.5$, $\mu = 1.0$, $\mu = 1.5$, $\mu = 2.0$) at excitation SPL of 140 dB

for large frequency ratio in Fig. 4(*a*) due to the interaction between the HR and compliant wall, two sharp TF resonant peaks can be noticed. Yet, for smaller frequency ratio $f = 0.01$, the two resonance peaks coalesce and the coupled HR is similar to a rigid HR. This is an evidence that the wall is not able to produce significant deflection because of an undesirable increase in stiffness of complaint wall compared to the stiffness of the resonator, so that the wall is insufficiently coupled with the air in the cavity. It is clear in Fig. 4(*a*) that the resonance provided by the HR with compliant wall is more broadband in TF amplitude than that of conventional rigid HR. Also, it can be clearly seen that the amplitudes of the two resonance peaks are not the same. With increasing the frequency ratio, regardless of mass ratio, the peak TF response of the first and second mode increases while the second peak shifts more. This means that via enhancing the deflection of the flexible wall, the amplitude of the pressure inside cavity increases while the mass of the system is unchanged which results in an increased capability for sound absorption of HR. With increasing the frequency ratio, the resonance frequency of both peaks reduces and the difference between the two resonance frequencies decreases.

Figure 4(*b*) presents that at the mass ratio of $\mu = 0.01$, the two TF resonant peaks for the 2DOF system merge into one peak, exhibiting that compliant wall does not cause significant changes in the response of the conventional HR. In the 2DOF system, the amplitude of first TF resonant peak is larger than that of conventional HR, suggesting that performance of HR can be enhanced by coupling with flexible wall in consequence to increased change in stiffness of system. With the increase of the mass ratio, the first resonance frequency decreases while the second resonance frequency increases, leading to an increased frequency gap between the two resonant peaks. This indicates the increased stiffness of cavity and thus an enhanced deflection of the flexible wall which is counteracted by the increase in air mass in the neck of the HR system. Also, as the mass ratio increases, the peak TF response of the first mode increases while the response of the second mode reduces. This is due to both decrease in the mass and enhanced deflection of the flexible wall. Accordingly, two comparable peaks in TF with small gap in-between can be obtained at desired frequencies through tuning the frequency ratio and a comparatively low mass ratio, which are set by the proper choice of the HR parameters as well as compliant wall material and geometrical properties.

5.4 Influences of Thickness and Material of Compliant Wall. Once a given material is chosen for the compliant wall, the strategic selection of the wall thickness can enable one to tailor the resonant modes of the compliant-walled HR. As a result, we explore the frequency dependence of the TF as a function of wall thickness in Fig. 5. The chosen parameters for HR are $a = 0.02$ m, $L = 0.035$ m, $V_1 = 0.0153$ m^3 and properties of aluminum wall are

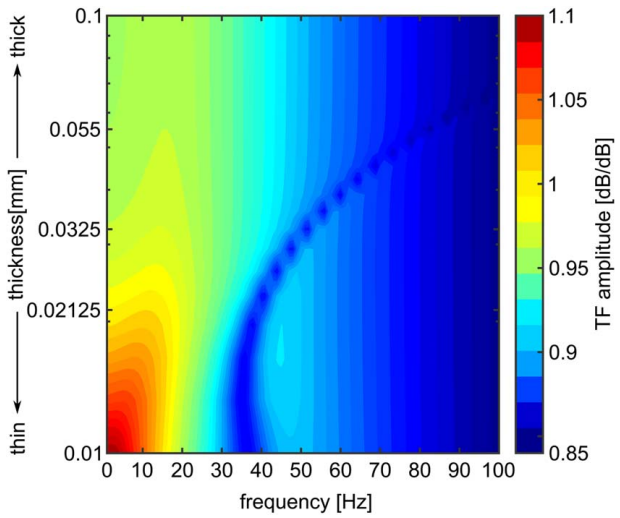

Fig. 5 Predictions of TF of a HR with compliant wall for 1–100 Hz and 0.01–0.1 mm wall thickness at excitation SPL of 140 dB. The cavity volume is 0.0153 m^3, the neck length is 0.035 m, and neck radius is 0.02 m.

mentioned in Table 2. In Fig. 5, the highest and lowest TF amplitude are 1.1 and 0.85, respectively. The resonance frequency of a rigid HR with the same physical dimensions is at 45 Hz at excitation SPL of 140 dB. For the HR with compliant wall, the 0.1 mm thick wall may be sufficiently rigid such that the wall material properties and thickness may not have considerable effect on the structural-acoustic modes in this low-frequency range of consideration. With decreasing the thickness of wall, the coupling between the wall and the HR cavity enhances and thus, a second resonance peak emerges and the first resonance frequency decreases. Using a 0.01 mm thick wall, the first resonance occurs at 2 Hz, exhibiting a significant shift from the resonance frequency of 45 Hz for rigid HR. Figure 5 also shows that with decreasing the thickness of wall, the frequency gap between the two resonant peaks first decreases and then increases. Accordingly, there is an optimal thickness where the frequency gap between the two resonance frequencies reaches a minimum, which is around 0.04 mm thickness of the compliant wall. This trend is due to interaction between (i) reduction in bending stiffness according to the cube of the wall thickness, and thus natural frequency of compliant wall and (ii) decreasing the mass of compliant wall. Decreasing the wall thickness increases the peak TF response of the first mode while the response of the second mode initially increases and then decreases due to the decrease in the mass and stiffness of flexible wall.

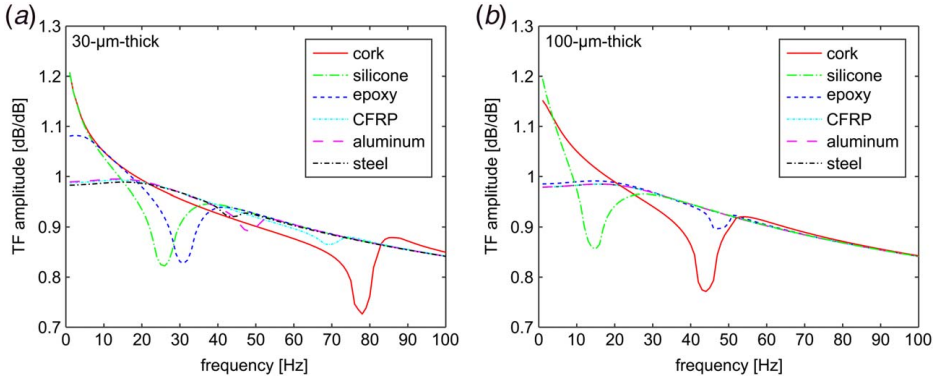

Fig. 6 Predictions of TF amplitude of a HR with compliant wall, showing the influences of change in material of compliant wall (cork, silicone, epoxy, CFRP, aluminum, or steel) at excitation SPL of 140 dB for 1–100 Hz and wall thickness of (*a*) $h = 30\ \mu$m and (*b*) $h = 100\ \mu$m. The cavity volume is 0.0153 m^3, the neck length is 0.035 m, and neck radius is 0.02 m.

The proper selection of wall material (i.e., Young's modulus, density, and Poisson's ratio) may lead to greater increase in the resulting acoustic energy absorption of the resonator. Thus, we leverage the model to investigate the influences of change in material of compliant wall having thickness of $h = 30\ \mu$m and $h = 100\ \mu$m on the TF, in Fig. 6. The materials considered are cork, silicone, epoxy, carbon fiber reinforced composite (CFRP), aluminum, and steel with the properties given in Table 2. In this selection, the modulus E of materials spans a factor of 20,000 from 0.01 GPa to more than 200 GPa; the density ρ spans a factor of 40 from less than 200 to more than 8000 kg/m^3. Cork has similar modulus as silicone, but the density of cork is considerably less than silicone. Thus, at the same thickness, the HR assembly with a compliant cork wall has lower frequency ratio, $f_{\text{cork}} < f_{\text{silicone}}$, and higher mass ratio, $\mu_{\text{cork}} > \mu_{\text{silicone}}$, than that of HR with silicone wall. As a result, as can be seen in Fig. 6(*a*), at wall thickness of $h = 30\ \mu$m, the resonance frequency of second TF resonant peak of HR assembly with cork is much lower than that of HR assembly with silicone wall. Also, due to their low modulus, for both materials, the first TF resonant peak is seen at very low frequency. Silicone, epoxy, and CFRP have roughly similar density, but the modulus of silicone is lower than that of epoxy, and modulus of epoxy is lower than that of CFRP. As a result, $f_{\text{CFRP}} < f_{\text{epoxy}} < f_{\text{silicone}}$ and $\mu_{\text{CFRP}} \approx \mu_{\text{cork}} \approx \mu_{\text{silicone}}$, leading to a greater TF resonant peak in HR with silicone than that of epoxy wall, and a higher TF resonant peak in HR with epoxy than that of CFRP wall. The resonance frequencies of HR with silicone are lower than that of epoxy wall and resonance frequency of HR with epoxy is lower than that of CFRP wall. Moreover, Fig. 6(*a*) presents that although aluminum and steel have high modulus and high density, at wall thickness of $h = 30\ \mu$m, these walls can notably affect the TF of HR assembly. Yet, among the 100-μm-thick walls, only cork, silicone, and epoxy walls are sufficiently compliant to influence the TF amplitude in this low-frequency range, as presented in Fig. 6(*b*). Thus, low-frequency sound attenuation can be obtained by judicious choice of compliant material parameters for wall. While much attention is placed on the potential beneficial nature of these materials as compliant wall, attention will also be given to possible limitations that could prevent the use of these materials or the plausibility of achieving the predicted results in real world environments. For instance, achieving a large displacement of a certain compliant wall material at low frequency 1–10 Hz when excited at 140 dB, fabrication of micron-thick wall, or assumption of material homogeneity in the model may be limiting factors that need to be considered in compliant-walled HR design.

6 Conclusions

This report investigates the nonlinear low-frequency response of a HR with a compliant wall in the nonlinear acoustic regime. The deflection of the compliant wall is exploited to couple with the HR dynamic mass to generate two low-frequency resonances and thus to enhance the sound attenuation capability of the HR. A reduced order model is established to characterize the salient acoustic-structure interaction mechanisms in the 2DOF system. A modeling case study is experimentally validated and examined to uncover how the lowest order resonant frequency of the 2DOF HR system is lower than that of the conventional rigid wall HR, including for increasingly nonlinear excitation SPLs. It is also found that the compliant wall enhances the TF of the HR cavity pressure to the external pressure and provides two low-frequency resonances associated with the 2DOF modes, albeit in a nonlinear regime. This research uncovers strategies of HR system design that have a significant influence on the nonlinear acoustic behavior of HR.

Acknowledgment

This research is supported in part by the National Science Foundation Faculty Early Career Development Award (No. 1749699) and in part by the Ford Motor Company.

Conflict of Interest

There are no conflicts of interest.

Data Availability Statement

The datasets generated and supporting the findings of this article are obtained from the corresponding author upon reasonable request. The authors attest that all data for this study are included in the paper.

References

[1] Berglund, B., Hassmén, P., and Job, R., 1996, "Sources and Effects of Low-Frequency Noise," J. Acoust. Soc. Am., **99**(5), p. 2985.
[2] Broner, N., 1978, "The Effects of Low Frequency Noise on People—A Review," J. Sound Vib., **58**(4), pp. 483–500.
[3] Horowitz, S., Nishida, T., Cattafesta, L., III, and Sheplak, M., 2002, "Characterization of a Compliant-Backplate Helmholtz Resonator for an Electromechanical Acoustic Liner," Int. J. Aeroacoust., **1**(2), pp. 183–205.
[4] Cui, S., and Harne, R., 2019, "Soft Materials With Broadband and Near-Total Absorption of Sound," Phys. Rev. Appl., **12**(6), p. 064059.
[5] Pan, W., Xu, X., Li, J., and Guan, Y., 2020, "Acoustic Damping Performance of Coupled Helmholtz Resonators With a Sharable Perforated Sidewall in the Presence of Grazing Flow," Aerosp. Sci. Technol., **99**, p. 105573.
[6] Tang, P., and Sirignano, W., 1973, "Theory of a Generalized Helmholtz Resonator," J. Sound Vib., **26**(2), pp. 247–262.
[7] Tang, S., 2005, "On Helmholtz Resonators With Tapered Necks," J. Sound Vib., **279**(3–5), pp. 1085–1096.
[8] Selamet, A., and Lee, I., 2003, "Helmholtz Resonator With Extended Neck," J. Acoust. Soc. Am., **113**(4), pp. 1975–1985.

[9] Cai, C., Mak, C., and Shi, X., 2017, "An Extended Neck Versus a Spiral Neck of the Helmholtz Resonator," Appl. Acoust., **115**, pp. 74–80.
[10] Selamet, A., Xu, M., Lee, I., and Huff, N., 2005, "Helmholtz Resonator Lined With Absorbing Material," J. Acoust. Soc. Am., **117**(2), pp. 725–733.
[11] Liu, F., Horowitz, S., Nishida, T., Cattafesta, L., and Sheplak, M., 2007, "A Multiple Degree of Freedom Electromechanical Helmholtz Resonator," J. Acoust. Soc. Am., **122**(1), pp. 291–301.
[12] Abbad, A., Rabenorosoa, K., Ouisse, M., and Atalla, N., 2018, "Adaptive Helmholtz Resonator Based on Electroactive Polymers: Modeling, Characterization, and Control," Smart Mater. Struct., **27**(10), p. 105029.
[13] Sugimoto, N., Masuda, M., and Hashiguchi, T., 2003, "Frequency Response of Nonlinear Oscillations of Air Column in a Tube With an Array of Helmholtz Resonators," J. Acoust. Soc. Am., **114**(4), pp. 1772–1784.
[14] Kim, S., Kim, Y., and Jang, J., 2006, "A Theoretical Model to Predict the Low-Frequency Sound Absorption of a Helmholtz Resonator Array," J. Acoust. Soc. Am., **119**(4), pp. 1933–1936.
[15] Cheng, Y., Xu, J., and Liu, X., 2008, "Broad Forbidden Bands in Parallel-Coupled Locally Resonant Ultrasonic Metamaterials," Appl. Phys. Lett., **92**(5), p. 051913.
[16] Seo, S., and Kim, Y., 2005, "Silencer Design by Using Array Resonators for Low-Frequency Band Noise Reduction," J. Acoust. Soc. Am., **118**(4), pp. 2332–2338.
[17] Tang, S., Ng, C., and Lam, E., 2012, "Experimental Investigation of the Sound Absorption Performance of Compartmented Helmholtz Resonators," Appl. Acoust., **73**(9), pp. 969–976.
[18] Hu, G., Tang, L., and Cui, X., 2019, "On the Modelling of Membrane-Coupled Helmholtz Resonator and Its Application in Acoustic Metamaterial System," Mech. Syst. Signal Process., **132**, pp. 595–608.
[19] Griffin, S., Lane, S., and Huybrechts, S., 2001, "Coupled Helmholtz Resonators for Acoustic Attenuation," ASME J. Vib. Acoust., **123**(1), pp. 11–17.
[20] Ruan, D., and Zhang, E., 2014, "Effect of Compliant-Diaphragm Geometry on the Transmission Loss Characteristics of Helmholtz Resonators," Noise Vib. Worldwide, **45**(11), pp. 9–15.
[21] Nudehi, S., Duncan, G., and Farooq, U., 2013, "Modeling and Experimental Investigation of a Helmholtz Resonator With a Flexible Plate," ASME J. Vib. Acoust., **135**(4), p. 041102.
[22] Cui, S., and Harne, R., 2020, "Acoustic-Structure Interaction in an Adaptive Helmholtz Resonator by Compliance and Constraint," ASME J. Vib. Acoust., **142**(2), p. 021005.
[23] Yu, G., Zhang, Y., and Shen, Y., 2011, "Nonlinear Amplitude-Frequency Response of a Helmholtz Resonator," ASME J. Vib. Acoust., **133**(2), p. 024502.
[24] Gourdon, E., Ture Savadkoohi, A., and Alamo Vargas, V., 2018, "Targeted Energy Transfer From One Acoustical Mode to an Helmholtz Resonator With Nonlinear Behavior," ASME J. Vib. Acoust., **140**(6), p. 061005.
[25] Vargas, V., Gourdon, E., and Savadkoohi, A., 2018, "Nonlinear Softening and Hardening Behavior in Helmholtz Resonators for Nonlinear Regimes," Nonlinear Dyn., **91**(1), pp. 217–231.
[26] Keller, J., and Zauner, E., 1995, "On the Use of Helmholtz Resonators as Sound Attenuators," Z. Angew. Math. Phys., **46**(3), pp. 297–327.
[27] Boullosa, R., and Orduña-Bustamante, F., 1992, "The Reaction Force on a Helmholtz Resonator Driven at High Sound Pressure Amplitudes," Am. J. Phys., **60**(8), pp. 722–726.
[28] Achilleos, V., Richoux, O., and Theocharis, G., 2016, "Coherent Perfect Absorption Induced by the Nonlinearity of a Helmholtz Resonator," J. Acoust. Soc. Am., **140**(1) pp. EL94–EL100.
[29] Singh, D., and Rienstra, S., 2014, "Nonlinear Asymptotic Impedance Model for a Helmholtz Resonator Liner," J. Sound Vib., **333**(15), pp. 3536–3549.
[30] Kinsler, L., Frey, A., and Coppens, A. S. J., 2000, *Fundamentals of Acoustics*, Wiley, New York.
[31] Virgin, L. N., 2007, *Vibration of Axially Loaded Structures*, Cambridge University Press, Cambridge.
[32] Leissa, A. W., 1969, *Vibration of Plates*, Scientific and Technical Information Division, National Aeronautics and Space Administration, Washington, DC.
[33] Leissa, A., 1973, "The Free Vibration of Rectangular Plates," J. Sound Vib., **31**(3), pp. 257–293.
[34] Dickey, N., Selamet, A., and Novak, J., 2000, "The Effect of High-Amplitude Sound on the Attenuation of Perforated Tube Silencers," J. Acoust. Soc. Am., **108**(3), pp. 1068–1081.
[35] Kela, L., 2009, "Resonant Frequency of an Adjustable Helmholtz Resonator in a Hydraulic System," Arch. Appl. Mech., **79**(12), pp. 1115–1125.